High Heat Flux Two-Phase Cooling of Electronics with Integrated Diamond/Porous Copper Heat Sinks and Microfluidic Coolant Supply

James W. Palko, Hyoungsoon Lee, Damena D. Agonafer, Chi Zhang, Ki Wook Jung, Jess Moss, Joshua D. Wilbur, Tom J. Dusseault, Michael Barako, Farzad Houshmand, Guoguang Rong, Tanmoy Maitra, Catherine Gorle, Yoonjin Won, Mehdi Asheghi, Juan G. Santiago, Kenneth E. Goodson
Department of Mechanical Engineering
Stanford University
440 Escondido Mall
Stanford, CA, USA, 94305

Derrick Rockosi, Ihor Mykyta, Dan Resler, David Altman
Advanced Technology Programs
Raytheon Integrated Defense Systems
Sudbury, MA, USA

Email: James.Palko@stanford.edu

ABSTRACT

We here present an approach to cooling of electronics requiring dissipation of extreme heat fluxes exceeding 1 kW/cm^2 over ~1 cm^2 areas. The approach applies a combination of heat spreading using laser micromachined diamond heat sinks; evaporation/boiling in fine featured (5 μm) conformal porous copper coatings; microfluidic liquid routing for uniform coolant supply over the surface of the heat sink; and phase separation to control distribution of liquid and vapor phases. We characterize the performance of these technologies independently and integrated into functional devices. We report two-phase heat transfer performance of diamond/porous copper heat sinks with microfluidic manifolding at full device scales (0.7 cm^2) with heat fluxes exceeding 1300 W/cm^2 using water working fluid. We further show application of hydrophobic phase separation membranes for phase management with heat dissipation exceeding 450 W/cm^2 at the scale of a single extended surface (~300 μm).

KEY WORDS: Two-phase cooling, high heat flux, diamond, porous copper, microfluidics

NOMENCLATURE

K	membrane gas permeance, Pa s/m
Q	volumetric flow rate, m^3/s
R	electrical resistance, Ω
T	temperature, K
h	heat transfer coefficient, W/m^2/K
k	thermal conductivity, W/m/K
p	pressure, Pa
q''	heat flux, W/m^2
u	velocity, m/s

Greek symbols
Δ	difference
κ	permeability, m^2

Subscripts
max	maximum

INTRODUCTION

Heat flux demands for electronics cooling have increased dramatically in recent years. A large number of electronic devices are capable of higher performance but are currently limited from achieving their intrinsic potential due to the inability to dissipate required heat loads. Examples include microwave amplifiers,[1] power transistors in inverters for renewable power generation and electric vehicle applications,[2] and 3D integrated microelectronics.[3] A number of cooling technologies have been developed to address this problem.[4], [5] Among these, two-phase liquid/vapor cooling approaches are particularly attractive due to the high heat transfer coefficients attainable and the large power dissipations facilitated by the latent heat of vaporization of the working fluid.

DARPA's Intrachip/Interchip Enhanced Cooling (ICECool) fundamentals program seeks to dramatically increase the heat dissipation capabilities of electronics cooling solutions by applying aggressive liquid/vapor phase change cooling technologies.[6] The goals of this program include dissipating heat fluxes in excess of 1 kW/cm^2 over large areas and heat fluxes of 5 kW/cm^2 at hot spots (e.g. 200 μm x 200 μm) relevant for electronics. Exit qualities exceeding 90% are targeted.

HEAT SINK DEVICE DESIGN

We combine a number of novel technologies in integrated devices to address the challenging goals of the ICECool fundamentals program:

1.) Laser micromachined polycrystalline diamond forms extended surfaces for heat spreading with area enhancements reaching 3:1. This dramatically reduces the heat fluxes that must be dissipated at the surface of the heat sink. The high thermal conductivity (e.g. 1500 W/m/K) provided by polycrystalline diamond allows high efficiencies for the extended surfaces even with the extremely high heat transfer coefficients obtained by boiling.

2.) We tightly integrate thin (<30 μm) porous copper layers conformally on the surfaces of the diamond heat spreader using templated electrodeposition allowing precise definition of the porous layer microstructure. The porous copper provides

low resistance paths for liquid delivery and thermal transport to evaporation surfaces, and provides large internal surface areas for heat removal by boiling and evaporation.

3.) 3D microfluidic routing provides uniform liquid delivery across heat spreaders with large area (1 cm^2). 3D manifolding minimizes liquid transport length, allowing adequate liquid supply to fine featured (5 μm) porous structures and facilitating thin porous layers with high internal surface area.

4.) We control the distribution of phases using phase separation layers which allow vapor escape while retaining liquid in the porous layer. The phase separation functionality allows pressure driven flow beyond the capillary driven component which generally limits achievable heat fluxes in phase change cooling solutions applying porous media. Furthermore, phase separation imposes explicit paths for liquid supply and vapor escape eliminating the competition between these processes.

Fig. 1 shows a schematic of the integrated device. Large heat fluxes in excess of 1 kW/cm^2 are supplied from the bottom of the heat sink, while coolant is pumped from the top. For the current device, water is used as the working fluid. We describe the implementation of each of the component technologies below.
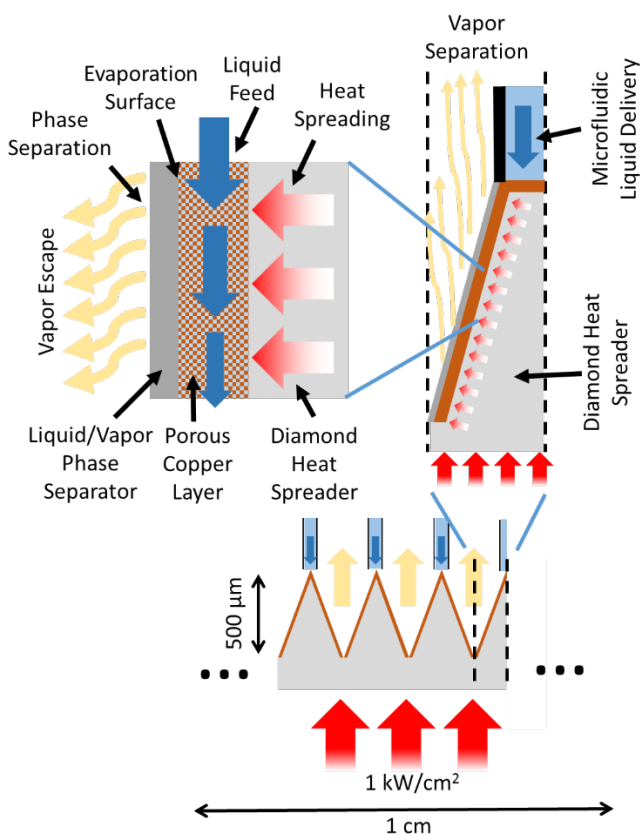

Fig. 1 Schematic of integrated diamond/porous copper heat sink with microfluidic coolant supply and phase separation for dissipation of extreme heat fluxes in excess of 1 kW/cm^2 over large areas, ~1 cm^2.

Diamond Heat Spreader

The diamond heat spreaders are laser micromachined[7] using a 1064nm Nd:YAG laser (US Laser Corp) from chemical vapor deposition (CVD) grown diamond dies (TM200, Element Six) with thickness of 700 μm. The thermal conductivity of this material exceeds 1500 W/m/K at the temperatures of interest (e.g. 400 K) [8] providing high efficiencies for the extended surfaces even with the high heat transfer coefficients obtained by boiling on enhanced surfaces. Fig. 2 shows micrographs of laser micromachined heat spreaders along with integrated porous copper layers discussed below. Stage temperature, O$_2$ flow rate, current (power), scan rate (mm/s) and number of passes per channel were varied to shape heat spreaders for maximum surface area enhancement and convenient interface to microfluidic manifolding. Residual ablated carbon was removed via annealing in an O$_2$ environment at elevated temperature (375°C), with results confirmed via visual inspection and Raman Spectroscopy. Heat spreaders have been fabricated with base to surface area enhancements up to ~ 3:1.
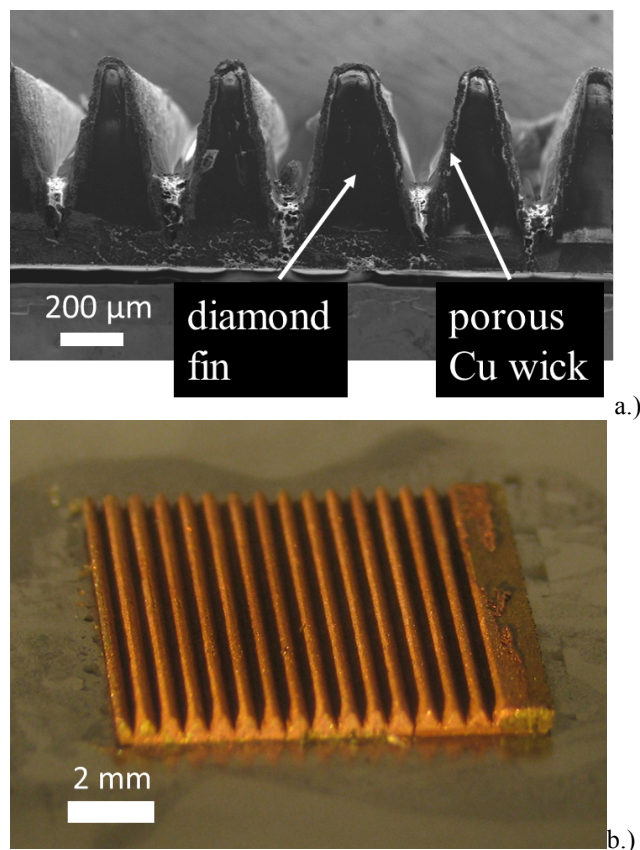

Fig. 2 Laser micromachined diamond heat spreaders with integrated conformal porous copper wick. a.) SEM micrograph of heat spreader with surface to base area enhancement ratio ~3:1. b.) Optical micrograph of heat spreader with surface to base area enhancement ratio ~1.5:1.

Porous Copper

Porous coatings provide a highly effective means of enhancing heat transfer in boiling[9], [10] and evaporation. We have fabricated porous copper on the extended surface of the diamond heat spreaders to maximize heat transfer coefficient and heat flux dissipation capability. The porous copper is conformally coated on the surface of the diamond heat spreader (Fig. 2) using electrodeposition around a sacrificial template as

has been described previously.[11], [12] Here we use a sacrificial template of polystyrene spheres, which are packed dry into the channels of the heat spreader. The spheres are then sintered to form necks between the particles. These necks correspond to channels between the pores in the inverse structure formed by electrodeposition around the template. This process allows tuning of permeability of the porous copper structure, with permeabilities exceeding 1e-12 m^2.[13] Fig. 3 shows a micrograph of the resulting porous copper structure. The resulting structure has characteristic pore sizes around 5 μm. The porous copper structures fabricated in this way also have high thermal conductivity (k = 170 W/m/K).[11] The effectiveness of these fine featured porous copper structures to dissipate extreme heat fluxes over small areas has been previously demonstrated.[14] Heat fluxes exceeding 1200 W/cm^2 have been dissipated using water working fluid with superheat less than 10 K, but this performance relies on short transport lengths (e.g. 150 μm).
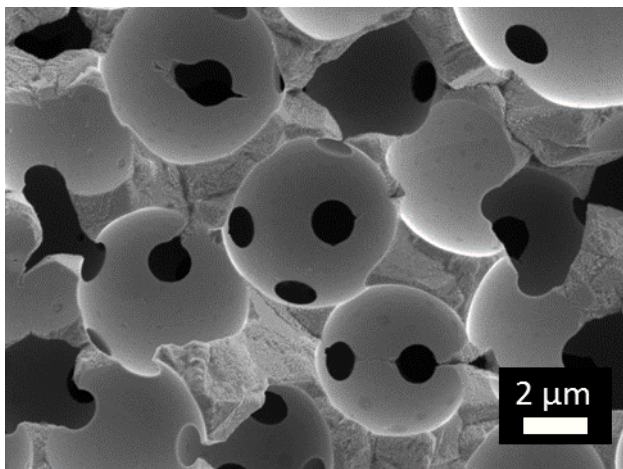
Fig. 3 SEM micrograph of porous copper structure produced by electrodeposition around sacrificial templates.

3D Microfluidic Routing

As demonstrated previously, small feature sizes can greatly increase the heat transfer coefficient of porous layers for boiling enhancement by creating large internal surface area.[14] However, small feature sizes dramatically reduce the permeability of the structures. In order to maximize total heat dissipation capability, it is, therefore, necessary to minimize the transport distances for liquid coolant. In order to preserve the performance of the porous copper that has been shown at small scale but allow cooling over areas relevant to electronics (e.g. 1 cm^2), we use microfluidic 3D routing of coolant to evenly supply liquid coolant to the surface of the heat sink. The manifold reduces the transport distance for liquid supply to the feature size of the extended surfaces (e.g. ~500 μm) and decouples this transport distance from the cooled area dimensions (e.g. ~1 cm). The effectiveness of 3D microfluidic manifolds for heat transfer applications has been demonstrated previously.[15]

A variety of fabrication methods are available for the production of 3D microfluidic manifolds including microfabrication[15] and high resolution 3D printing. We fabricated the current manifold from a series of layers which

either supply liquid to the heat sink surface or allow vapor to escape from it (Fig. 4a). The layers are formed from polyimide films, which are cut to shape using laser ablation. Vapor escape layers consist of films (125 μm thick) cut to form an open mesh to allow vapor venting, while liquid supply layers are formed by a layer (50 μm thick) with laser cut microchannels (500 μm wide) which direct liquid to the heat sink surface (Fig. 4b) sandwiched between thin (25 μm) continuous films which contain liquid in the channels. Liquid is supplied to the microchannels of the liquid delivery layer by two liquid supply headers that penetrate both the liquid deliver and vapor escape layers outside of the cooled area. The microchannels individually route liquid from the headers to the heat sink surface, guaranteeing uniform liquid distribution over the heat sink surface without. Four vapor escape layers and a single liquid delivery layer are stacked in each channel of the heat spreader (Fig. 4c). The layers are shifted vertically with respect to each other to conform to the contours of the heat spreader. Using this configuration, liquid may be introduced at the top or bottom of the channel. For the large scale (0.7 cm^2) heat transfer experiments reported below, liquid is introduced to the bottom of the heat sink channel.
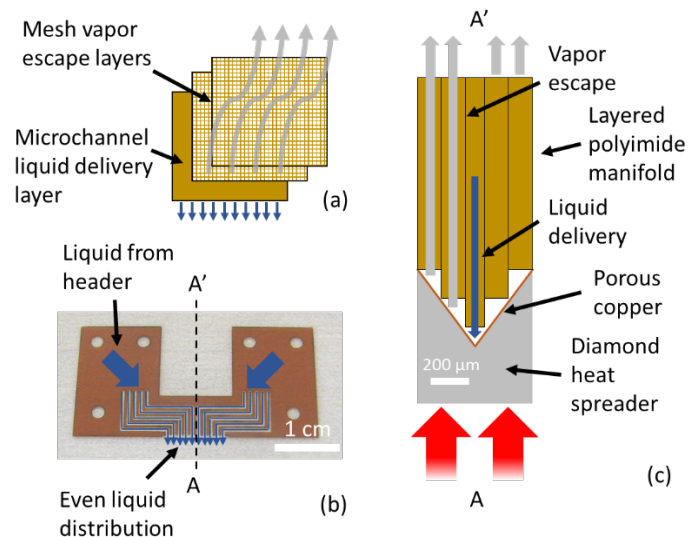
Fig. 4 3D microfluidic manifold for routing of coolant to heat sink surface. a.) Manifold is formed from stack of open mesh vapor escape layers and liquid delivery layers containing microchannels which route liquid to the heat sink surface. b.) Core of liquid delivery layer with laser cut microchannels which individually route liquid to the heat sink surface. Liquid is contained within the microchannels by continuous films sandwiching the core. c.) Cross section of single heat sink channel and manifold supplying liquid to channel base.

Phase Separation

The diamond heat spreader, conformal porous copper surface enhancement, and 3D microfluidic routing manifold have been integrated to produce a device capable of dissipating high heat flux ($q'' > 1300$ W/cm^2) over large areas (0.7 cm^2) as discussed below. However, balancing adequate liquid supply while minimizing flooding is difficult in such a device. Phase separation allows supply of the liquid with driving pressures

exceeding those available with capillary action alone while avoiding flooding of the heat sink which restricts vapor escape. Phase separation has been applied previously to reduce pressure drop incurred in flow boiling.[16], [17]

The use of water as a working fluid allows efficient phase separation using porous hydrophobic materials. We have applied expanded polytetrafluoroethylene (ePTFE) membranes with thickness of ~10 μm (Zeus, INFO) to retain liquid in porous copper layers while venting vapor produced by boiling. The most significant characteristic of phase separation membranes applied in this context is resistance to gas escape. We have measured the gas permeance[18] of the ePTFE membranes

$$K = \frac{u}{\nabla p} \qquad (1)$$

using room temperature air flows with velocity u = 0.83 m/s. The measured permeance is 0.21 m/s/kPa. The stand-alone nature of the phase separation membrane allows integration with the layered microfluidic manifold described previously. We are also exploring porous hydrophobic coatings that can be deposited in place and adhere directly to the porous copper.

COMPONENT AND DEVICE PERFORMANCE

We have characterized the performance of the individual components discussed above as well as their integrated combinations.
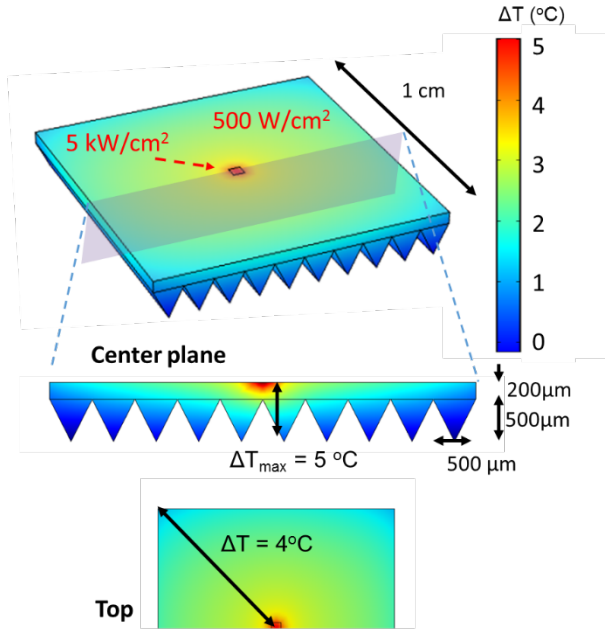

Fig. 5 Heat spreading in diamond heat sink with 2.2:1 surface to base area enhancement ratio. 500 W/cm^2 heat flux is applied to the entire 1 cm^2 heated area while a heat flux of 5 kW/cm^2 is applied to the 0.04 mm^2 hot spot at the center of the heat spreader. A constant heat transfer coefficient h = 50 kW/m^2 K is applied on the extended surfaces. Temperature rise above minimum surface temperature is shown.

Heat Spreading

We simulated the capability of the diamond heat spreader to distribute large base and hot spot heat fluxes to the extended surfaces with minimal temperature gradients. Fig. 5 shows the temperature distribution in a diamond heat spreader under example operating conditions. The heat spreader has a 1 cm x 1 cm heated area with a 200 μm x 200 μm localized hot spot at the center of the device. Triangular channels have a depth of 500 μm and a spacing of 500 μm, giving a surface to base area enhancement ratio of 2.2:1. The total thickness of the heat spreader is 700 μm. 500 W/cm^2 heat flux is applied over the entire heated area with 5 kW/cm^2 heat flux at the hot spot. A constant heat transfer coefficient of h = 50 kW/m^2 K is applied on the extended surfaces. Simulations were performed in COMSOL Multiphysics with 1.1 million tetrahedral mesh elements. Temperature differences from the hotspot to the heat sink surface are less than 5 K, while temperature differences across the heated area are less than 4 K.

Large Area Heat Transfer Performance

The effective heat spreading provided by diamond can be combined with the previously demonstrated[14] extreme heat flux dissipation capability and large heat transfer coefficients provided by the fine featured, electrodeposited porous copper to cool large areas (e.g. 1 cm^2) when applied with microfluidic manifolding to minimize liquid transport distances. We have characterized the heat transfer performance of the integrated porous copper/diamond heat sink in boiling using low pressure liquid feed with water as the working fluid as shown schematically in Fig. 6.
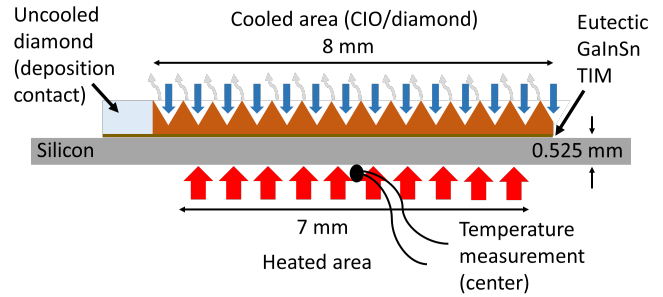

Fig. 6 Heat transfer performance characterization experiment for integrated diamond/porous copper heat sinks in boiling with 3D microfluidic liquid supply.

Heat is supplied to the heat spreader through a silicon substrate with a thin film (100 nm) platinum heater deposited on the opposite side. The heated area is 7 mm x 10 mm. Due to the high heat fluxes required, the thermal interface between the silicon substrate and diamond is key to conducting and interpreting heat transfer experiments in this configuration. Eutectic GaInSn (Galinstan, Geratherm Medical AG) is used as a thermal interface material (TIM). It has good thermal conductivity, k = 27.6 W/m/K[19] with excellent accommodation of roughness of the diamond or silicon surfaces. Given the large lateral extent of the heater compared to the silicon substrate thickness (~13 X) and high heat transfer coefficient provided by the diamond heat spreader, we expect spreading to be limited to the edges of the heater. The heat flux near the center of the heater, where temperature is measured by a thermocouple, is transmitted directly to the heat spreader without significant reduction. Liquid water at room temperature is supplied to the base of the heat sink channels

using the 3D microfluidic manifold, and vapor is allowed to vent to ambient.

The combination of heat spreading by diamond, boiling heat transfer performance of fine featured electrodeposited copper, and uniform liquid distribution via 3D microfluidic manifolding allows dissipation of extreme heat fluxes of more than 1300 W/cm^2 at the heated surface. Fig. 7 shows the heat flux, *q"*, at the heated surface as a function of diamond base temperature calculated from the heater centerline temperature. Two different liquid flow rates of Q = 3.08 and 0.96 ml/s were tested, showing critical heat flux (CHF) values of 1341.6 and 823.6 W/cm^2 respectively, as determined at the heater surface.

Temperature is measured at the center of the heated surface. Determination of temperature at the bottom of the diamond heat spreader requires correction for temperature loss due to conduction from the heater surface to the diamond surface. We have calculated the temperature drop across the silicon substrate accounting for the temperature dependence of its thermal conductivity.[20] Fig. 7 shows calculated temperature at the diamond base for negligible liquid metal TIM thickness and a thickness of 10 μm.

Inlet feed pressures for the 3.08 and 0.96 ml/s flow rate experiments, were 42.1 kPa and 15.9 kPa, respectively. Based on the supplied heat fluxes, these correspond to coefficients of performance (CoP) of ~7,000 and ~37,000, respectively.
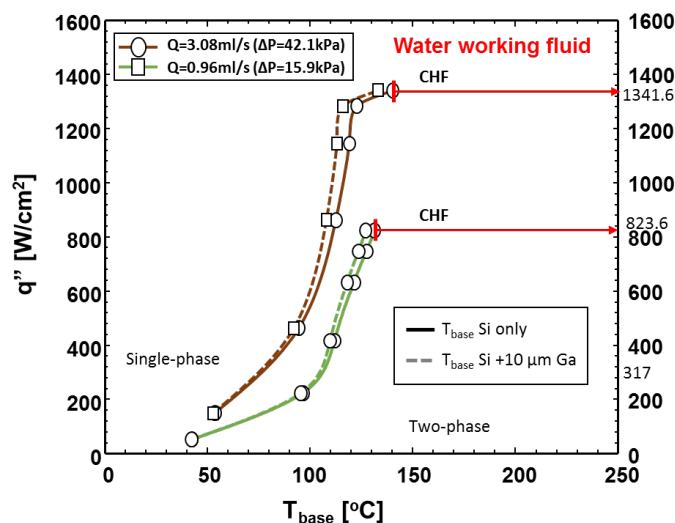

Fig. 7 Two-phase heat transfer performance for integrated diamond/porous copper heat sink with 3D microfluidic manifolding and 0.7 cm^2 heated area using water working fluid. Heat flux at heater surface is plotted versus temperature at the base of the heat sink calculated based on the heater temperature and accounting for conduction through the silicon substrate and TIM. Separate conduction calculations were performed assuming both negligible TIM thickness (solid lines) and 10 μm thick TIM.

Two-phase Heat Transfer with Phase Separation at Small Scale

We have demonstrated the use of hydrophobic membranes to explicitly separate vapor and liquid phases during boiling heat transfer at small scale (0.6 mm^2). These experiments use

a small active region which is volumetrically Joule heated by passing a current through the porous copper. Fig. 8 shows a schematic of the small scale experiment characterizing phase separation heat transfer performance.
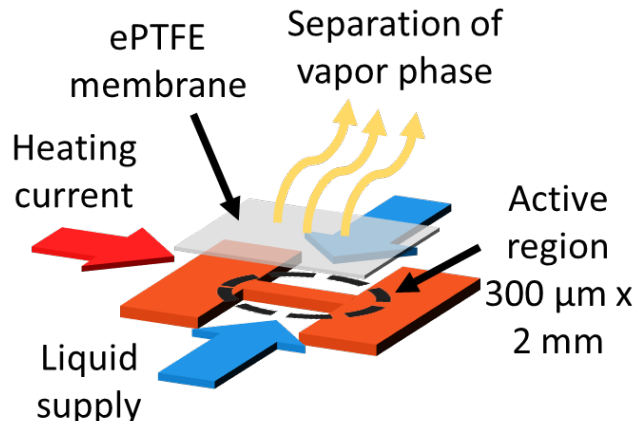

Fig. 8 Small scale phase separation heat transfer characterization schematic.

The active region is 30 μm thick porous copper fabricated as described above and is supported on a polyimide film. The active region is formed by laser ablation from a larger planar porous copper/polyimide bilayer (Fig. 9).
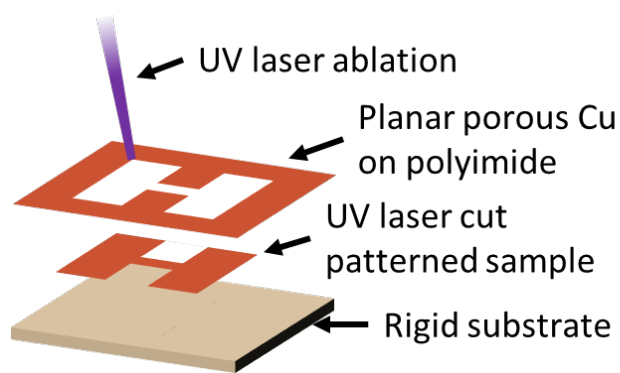

Fig. 9 Small scale heat transfer sample fabrication. The active region is laser cut from uniform planar porous Cu layer previously grown on thin polyimide substrate. The sample is then adhered to a rigid acrylic substrate.

Fig. 10 shows a micrograph of a small scale heat transfer sample. The active region connects to two large pads also formed of porous copper that supply current while minimizing heating outside of the active region. Liquid is delivered under pressure to the bridge via ports cut in the rigid substrate to which the polyimide/porous copper bilayer is adhered with epoxy. The porous copper is covered by a 10 μm thick ePTFE membrane pressed on to the active region by a 50 μm thick polyimide film with multiple 200 μm x 400 μm windows cut through it to allow vapor escape (Fig. 11). This film is further reinforced by a 125 μm thick polyimide film with a 2.5 mm x 0.5 mm window. Sealing is provided by silicone gasket material.
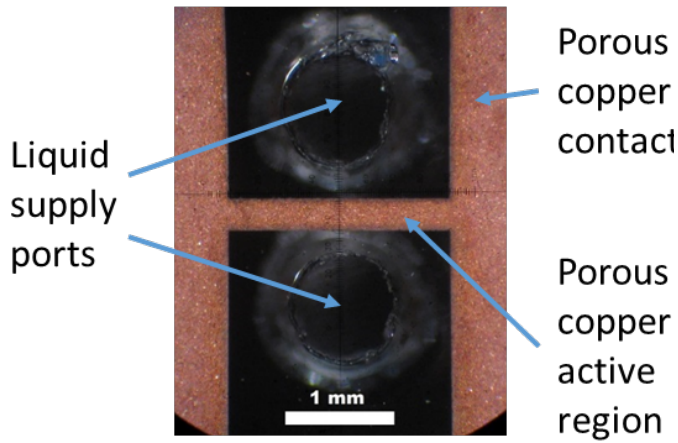
Fig. 10 Small-scale phase separation experimental sample. Liquid is delivered out of the page from the ports in the substrate to the porous copper active region that is heated by passing current.
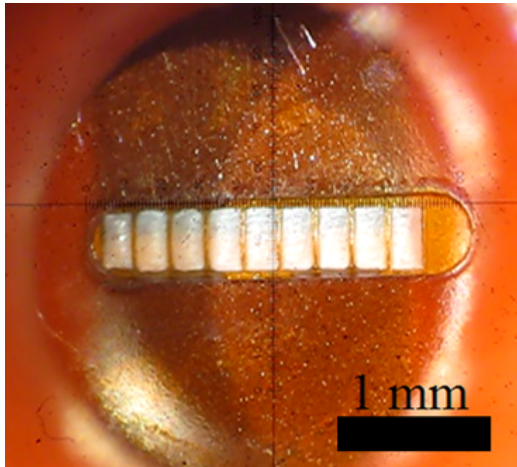

Fig. 11 ePTFE phase separation membrane (white) covering active region of small-scale heat transfer device shown in Fig. 10. 50 μm thick polyimide film (amber), with 200 μm x 400 μm windows cut through it to allow vapor escape, holds the membrane against the active region. 125 μm thick polyimide film, with a 500 μm x 2.5 mm window provides further reinforcement.

The active region provide electrical resistance of R = 24.3 mΩ. We determine active region temperature using electrical resistance thermometry[21] with a four-point measurement across the active region itself as the resistive element. Measured temperature represents an average value based on the net electrical resistance of the entire active region. The temperature coefficient of resistivity for porous copper grown using this technique has been characterized previously and found to be 3.857 + 0.002 x 10-3 K^{-1},[14] similar to that reported for bulk Cu.[22] Systematic errors for both active region temperature and power dissipation measurements during heat transfer experiments were estimated to be 1%.
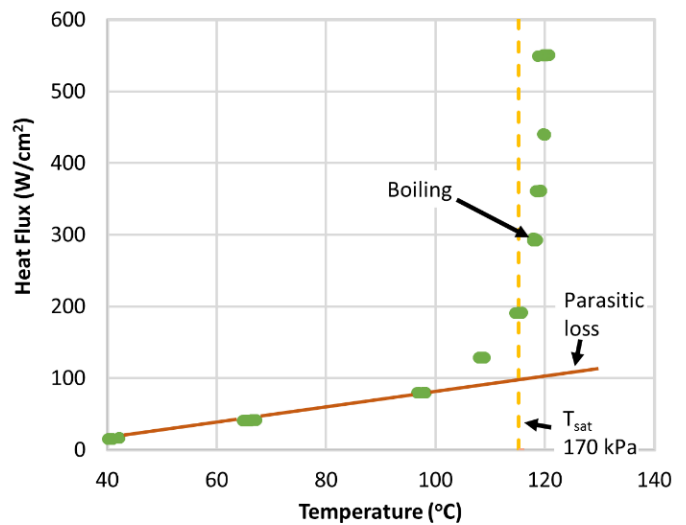

Fig. 12 Heat transfer performance for small scale (0.6 mm^2) porous copper active region with phase separation and 69 kPa pressurized feed of water. Measured active region heat flux and temperature are shown (symbols). Parasitic conduction loss is determined based on low temperature thermal resistance of the active region and indicated by the brown solid line. Saturation temperature at inlet feed pressure is indicated by the vertical dashed line.

Fig. 12 shows the power density dissipated by the small scale platform versus active region temperature, with phase separation and water feed pressurized to 69 kPa. The active region supports power densities up to 550 W/cm^2 before burn-out with a nearly constant temperature at high heat fluxes of ~120 ^{o}C. Parasitic conduction losses for the small scale experimental configuration can be determined from the low power region of the curve shown in Fig. 12 indicating ~ 100 W/cm^2 of power dissipation is due to conduction at 120 ^{o}C. More than 450 W/cm^2 of power dissipation is attributable to phase change.

The maximum recorded heat flux corresponds to burn out of the active region. Based on post-test microscopic analysis, however, we believe this is due to thermal failure of the polymer substrate structure, not loss of cooling in the active region. Therefore, the maximum recorded heat flux is likely not representative of the critical heat flux for the system.

SUMMARY & CONCLUSIONS

We have demonstrated two-phase cooling of extreme heat fluxes via the application of four technologies: heat spreading using laser micromachined diamond with exceptional thermal conductivity, enhanced boiling in fine featured porous copper fabricated using templated electrodeposition, uniform liquid supply over large areas using 3D microfluidic manifolding, and phase separation structures to control the distribution of liquid and vapor. We show the capability of these technologies to dissipate heat fluxes in excess of 1300 W/cm^2 over large areas (0.7 cm^2). The combination of these technologies provides opportunities for unprecedented performance in electronics cooling.

REFERENCES

[1] Y. Won, J. Cho, D. Agonafer, M. Asheghi, and K. E. Goodson, "Cooling Limits for GaN HEMT Technology," *Compound Semiconductor Integrated Circuit Symposium (CSICS), 2013 IEEE*. pp. 1–5, 2013.

[2] M. Andresen and M. Liserre, "Impact of active thermal management on power electronics design," *Microelectron. Reliab.*, vol. 54, no. 9–10, pp. 1935–1939, 2014.

[3] A. Bar-Cohen and K. J. L. Geisler, "Cooling the Electronic Brain," *Mech. Eng.*, no. April, pp. 38–41, 2011.

[4] K. P. Bloschock and A. Bar-Cohen, "Advanced thermal management technologies for defense electronics," *Proc. SPIE Vol*, vol. 8405, p. 84050I–84050I–12, 2012.

[5] I. Mudawar, "Assessment of high-heat-flux thermal management schemes," *Components and Packaging Technologies, IEEE Transactions on*, vol. 24, no. 2. pp. 122–141, 2001.

[6] A. Bar-Cohen, "Intrachip/Interchip Enhanced Cooling (ICECool)." [Online]. Available: http://www.darpa.mil/program/intrachip-interchip-enhanced-cooling.

[7] M. V Corbin, M. M. Debenedictis, D. B. James, S. P. Leblanc, and L. R. Paradis, "Diamond Microchannel Heat Sink Designs For High Heat Flux Thermal Control," *11th Annu. AIAA/MDA Technol. Conf.*, pp. 1–11, 2002.

[8] S. . Coe and R. . Sussmann, "Optical, thermal and mechanical properties of CVD diamond," *Diam. Relat. Mater.*, vol. 9, no. 9–10, pp. 1726–1729, 2000.

[9] R. P. Rioux, E. C. Nolan, and C. H. Li, "A systematic study of pool boiling heat transfer on structured porous surfaces: From nanoscale through microscale to macroscale," *AIP Adv.*, vol. 4, no. 11, p. 117133, 2014.

[10] M. Mccarthy, M. Rahman, and E. Olceroglu, "Role of Wickability on the Critical Heat Flux of Structured Superhydrophilic Surfaces," *Langmuir*, vol. 30, pp. 11225–11234, 2014.

[11] M. T. Barako, J. M. Weisse, S. Roy, T. Kodama, T. J. Dusseault, M. Motoyama, M. Asheghi, F. B. Prinz, Z. Xiaolin, and K. E. Goodson, "Thermal conduction in nanoporous copper inverse opal films," in *Thermal and Thermomechanical Phenomena in Electronic Systems (ITherm), 2014 IEEE Intersociety Conference on*, 2014, pp. 736–743.

[12] T. J. Dusseault, J. Gires, M. T. Barako, Y. Won, D. D. Agonafer, M. Asheghi, J. G. Santiago, K. E. Goodson, W. Yoonjin, D. D. Agonafer, M. Asheghi, J. G. Santiago, and K. E. Goodson, "Inverse opals for fluid delivery in electronics cooling systems," in *Thermal and Thermomechanical Phenomena in Electronic Systems (ITherm), 2014 IEEE Intersociety Conference on*, 2014, no. c, pp. 750–755.

[13] C. Zhang, G. Rong, J. W. Palko, T. J. Dusseault, M. Asheghi, J. G. Santiago, and K. E. Goodson, "No Title," in *ASME 2015 InterPACK Conference*, 2015.

[14] J. W. Palko, C. Zhang, J. D. Wilbur, T. J. Dusseault, M. Asheghi, K. E. Goodson, and J. G. Santiago, "Approaching the limits of two-phase boiling heat transfer: High heat flux and low superheat," *Appl. Phys. Lett.*, vol. 107, no. 25, p. 253903, 2015.

[15] Y. Won, E. N. Wang, K. E. Goodson, and T. W. Kenny, "3-D visualization of flow in microscale jet impingement systems," *Int. J. Therm. Sci.*, vol. 50, no. 3, pp. 325–331, Mar. 2011.

[16] M. P. David, J. E. Steinbrenner, J. Miler, and K. E. Goodson, "Adiabatic and diabatic two-phase venting flow in a microchannel," *Int. J. Multiph. Flow*, vol. 37, no. 9, pp. 1135–1146, 2011.

[17] M. P. David, J. Miler, J. E. Steinbrenner, Y. Yang, M. Touzelbaev, and K. E. Goodson, "Hydraulic and thermal characteristics of a vapor venting two-phase microchannel heat exchanger," *Int. J. Heat Mass Transf.*, vol. 54, no. 25–26, pp. 5504–5516, 2011.

[18] L. K. Massey, "1.2 Mass Transport of a Gas ," William Andrew Publishing/Plastics Design Library.

[19] S. Yu and M. Kaviany, "Electrical, thermal, and species transport properties of liquid eutectic Ga-In and Ga-In-Sn from first principles.," *J. Chem. Phys.*, vol. 140, no. 6, p. 064303, 2014.

[20] C. J. Glassbrenner and G. A. Slack, "Thermal Conductivity of Silicon and Germanium from 3\ifmmode^\circ\else\textdegree\fi{}K to the Melting Point," *Phys. Rev.*, vol. 134, no. 4A, pp. A1058–A1069, May 1964.

[21] P. R. N. Childs, "6 - Resistance temperature detectors," in *Practical Temperature Measurement*, P. R. N. B. T.-P. T. M. Childs, Ed. Oxford: Butterworth-Heinemann, 2001, pp. 145–193.

[22] R. A. Matula, "Electrical resistivity of copper, gold, palladium, and silver," *J. Phys. Chem. Ref. Data*, vol. 8, no. 4, 1979.